AD-A115 783 DAYTON UNIV OH SCHOOL OF ENGINEERING F/G 20/1
SOUND TRANSMISSION THROUGH DUCTS AND AIRCRAFT NOISE PREDICTION.--ETC(U)
JAN 82 J J SCHAUER, J T DATKO, R W GUYTON F33615-78-C-2016
UNCLASSIFIED UDR-TR-81-118 AFWAL-TR-81-2131-VOL-1 NL

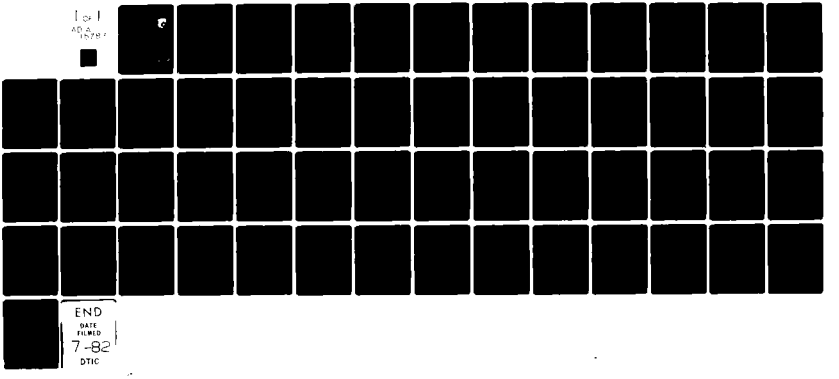

END
DATE FILMED
7-82
DTIC

(2)

AFWAL-TR-81-2131, Vol. I

SOUND TRANSMISSION THROUCH DUCTS AND AIRCRAFT NOISE PREDICTION VOLUME I - TECHNICAL REPORT

John J. Schauer
John T. Datko
Robert W. Guyton

School of Engineering
University of Dayton
Dayton, Ohio 45469

January 1982

FINAL REPORT 15 May 1978 - 15 May 1981

APPROVED FOR PUBLIC RELEASE; DISTRIBUTION UNLIMITED

AERO PROPULSION LABORATORY
AIR FORCE WRIGHT AERONAUTICAL LABORATORIES
AIR FORCE SYSTEMS COMMAND
WRIGHT-PATTERSON AIR FORCE BASE, OHIO 45433

NOTICE

When Government drawings, specifications, or other data are used for any purpose other than in connection with a definitely related Government procurement operation, the United States Government thereby incurs no responsibility nor any obligation whatsoever; and the fact that the government may have formulated, furnished, or in any way supplied the said drawings, specifications, or other data, is not to be regarded by implication or otherwise as in any manner licensing the holder or any other person or corporation, or conveying any rights or permission to manufacture use, or sell any patented invention that may in any way be related thereto.

This report has been reviewed by the Office of Public Affairs (ASD/PA) and is releasable to the National Technical Information Service (NTIS). At NTIS, it will be available to the general public, including foreign nations.

This technical report has been reviewed and is approved for publication.

James S Petty

JAMES S. PETTY
Project Engineer

Marvin F. Schmidt

MARVIN F. SCHMIDT
Acting Chief, Components Branch

FOR THE COMMANDER

James M. Shipman

JAMES M. SHIPMAN, Maj, USAF
Acting Director, Turbine Engine Division

"If your address has changed, if you wish to be removed from our mailing list, or if the addressee is no longer employed by your organization please notify AFWAL/POTC, *W-PAFB, OH 45433 to help us maintain a current mailing list".*

Copies of this report should not be returned unless return is required by security considerations, contractual obligations, or notice on a specific document.

Unclassified

SECURITY CLASSIFICATION OF THIS PAGE *(When Data Entered)*

REPORT DOCUMENTATION PAGE		READ INSTRUCTIONS BEFORE COMPLETING FORM
1. REPORT NUMBER AFWAL-TR-81-2131, Vol. I	2. GOVT ACCESSION NO. AD-A115 983	3. RECIPIENT'S CATALOG NUMBER
4. TITLE *(and Subtitle)* SOUND TRANSMISSION THROUGH DUCTS AND AIRCRAFT NOISE PREDICTION. VOLUME I - TECHNICAL REPORT		5. TYPE OF REPORT & PERIOD COVERED Final Report 15 May 78-15 May 1981
		6. PERFORMING ORG. REPORT NUMBER UDR-TR-81-118
7. AUTHOR(s) John J. Schauer John T. Datko Robert W. Guyton		8. CONTRACT OR GRANT NUMBER(s) F33615-78-C-2016
9. PERFORMING ORGANIZATION NAME AND ADDRESS School of Engineering University of Dayton Dayton, Ohio 45469		10. PROGRAM ELEMENT, PROJECT, TASK AREA & WORK UNIT NUMBERS Project 3066
11. CONTROLLING OFFICE NAME AND ADDRESS Air Force Aero Propulsion Laboratory (POTC) AF Wright Aeronautical Laboratories, AFSC Wright-Patterson AFB, OH 45433		12. REPORT DATE January 1982
		13. NUMBER OF PAGES 46 pages
14. MONITORING AGENCY NAME & ADDRESS*(if different from Controlling Office)*		15. SECURITY CLASS. *(of this report)* Unclassified
		15a. DECLASSIFICATION/DOWNGRADING SCHEDULE

16. DISTRIBUTION STATEMENT *(of this Report)*

Approved for public release; distribution unlimited.

17. DISTRIBUTION STATEMENT *(of the abstract entered in Block 20, if different from Report)*

18. SUPPLEMENTARY NOTES

19. KEY WORDS *(Continue on reverse side if necessary and identify by block number)*

Lining impedance	Sound propagation
Impedance models	Variable area ducts
Ray acoustics	Aircraft noise
Hydrodynamic modes	Noise prediction
Transient analysis	Mode orthogonality

20. ABSTRACT *(Continue on reverse side if necessary and identify by block number)*

Aircraft engine acoustical lining impedance models, ray acoustics, hydrodynamic modes, and transient analysis of sound propagation in variable area duct studies were applied to aircraft noise prediction. The effects of several duct lining configurations in a TF33 P5 and a CFM56 engined KC-135B aircraft were predicted. The prediction was based on a model corrected to fit flight noise data and modified by including theoretical duct noise attenuation predictions. The transient solution of variable area ducts

DD FORM 1 JAN 73 1473 EDITION OF 1 NOV 65 IS OBSOLETE

Unclassified

SECURITY CLASSIFICATION OF THIS PAGE *(When Data Entered)*

ABSTRACT (continued)

permitted the prediction of sound propagation in bullet nose inlets for no flow and was moderately successful when a potential flow was included with low Mach numbers. Volume I contains the technical report and analysis. Volume II contains the user's manuals and listings of the computer codes developed.

FOREWORD

This report summarizes the work done under Air Force Aero Propulsion Laboratory Contract No. F33615-78-C-2016 during the period of 11 November 1977 to 15 February 1981. It contains: (1) the changes made in the Air Force Propulsion Laboratory's noise/performance trade procedure, and (2) the analytical work describing the propagation of sound waves in variable area soft walled ducts with flow. Ducts of this type are found in the inlet and exhaust passages of high-bypass turbojet engines. This analytical work was used in developing computer programs predicting the attenuation of sound in these ducts. The programs are detailed in user manuals. The work was done by Dr. John J. Schauer, Mr. John T. Datko, Mr. Robert W. Guyton, Mr. David W. Ewick, Mr. Eugene P. Hoffman, and Mr. Robert N. Bergen of the University of Dayton under Project Engineers Mr. Robert M. McGregor and Dr. James S. Petty of the Aero Propulsion Laboratory, AFWAL/POTC, Wright-Patterson Air Force Base, Ohio 45433.

TABLE OF CONTENTS

TABLE OF CONTENTS (continued)

LIST OF ILLUSTRATIONS

LIST OF TABLES

SECTION I

INTRODUCTION AND SUMMARY

This work was a continuation of an investigation of aircraft duct acoustics which started at the University of Dayton in 1972. In this period the University of Dayton has aided the Air Force Aero Propulsion Laboratory in the highly analytical area of Duct Acoustics.

Under this most recent contract the effort was divided into two tasks. Task 1 consisted of a review and evaluation of duct acoustic models developed by others and published prior to or during this effort. Included in this task was maintenance of exiting Air Force noise programs and improvement or modification of these programs in the area of duct acoustics.

Task 2 was divided into three phases. Phase I consisted of sound transmission prediction in ducts. Of particular concern under this phase were the examination of sheared flow orthogonality theories previously studied and the variable area duct sound transmission problem. Phase II required the integration of previously developed models into the primary Air Force noise prediction program. Phase III ensured that the integrated changes worked and verified the resultant program by predicting noise for various duct lining configurations.

TASK 1 - RESULTS

A published lining design model was adopted as a part of the Propulsion Lab noise/performance trade methodology. The resultant program, based on the Boeing publication by Armstrong [1], is an improvement over the previous duct lining program because it includes in the model the effects of boundary layer thickness and local sound pressure level. It also models polymide sheet linings.

Another published technique was developed into an approximate method for estimating sound attenuation in lined ducts. The ray acoustics model published by Rice, Heidman and Sefrin [2] was the basis for this program. It was desirable because it produces an estimated value for the complex axial sound propagation constants associated with the duct modes. These are required as an initial guess by the eigenvalue finding program OPTSHE developed under a previous contract. Prior to this programs development, experience was the only basis for the initial guess required for OPTSHE and it was difficult to home in on the desired eigenvalue. The approximating program is also useful for finding a quick estimate for the more highly

attenuated modes which play only a minor role when the sound energy is distributed among all the propagating modes. This feature was utilized in the Task 2 equal energy work.

TASK 2 - RESULTS

As part of Phase I of this task, sound transmission in ducts was investigated. In particular orthogonality conditions in shear flow and transmission in variable area ducts was studied.

The sheared flow orthogonality proved to be difficult. Interactions of the acoustic field with the hydrodynamic field were evident. Progress in the uniform mean flow situation was good. Here, a clearly defined fluctuating hydrodynamic field was shown to fit the governing equations independent of the acoustical field. This hydrodynamic field travels down the duct at the speed of the uniform flow velocity. For rotational or sheared flow in a duct, several techniques were tried to produce a solution of the governing partial differential equations. No satisfactory results were obtained.

Variable area ducts were approached with a transient finite difference solution to the governing equations. The variable duct profile was mapped conformally into a rectangle. The resultant mapping was used to transform the governing equations in order that the finite difference grid could be set up on the rectangle. The resuts were very encouraging for the no flow conditions. With a irrotation mean flow, results were also obtained but not over the range of parameters of interest.

As part of Phase II of this task, the theoretical development of previous contractual efforts were integrated into the noise/performance program. Specifically, the least attenuation mode theory and the equal energy theoretical duct attenuation were included as options to the existing empirical duct attenuation prediction. In addition, the program was expanded to permit the results of any attenuation prediction to be input to the program.

Under Phase III the noise prediction program output was compared to flight data and corrections to the predicted noise were formulated for the KC-135B aircraft. Hard walled engine ducts and three soft walled ducts were evaluated for two different engines, the TF33-P5 and the CFM 56. The physical properties of the soft walls were found to enable the lining's effect on performance to be judged.

SECTION II

LINING IMPEDANCE MODELS

PERFORATED SHEET IMPEDANCE MODEL

The normalized resistance ($R/\rho c$) and normalized reactance ($X/\rho c$) can be calculated for a perforated sheet acoustic lining material, using Fortran IV Subroutines ENGNOR and METNOR. The former works entirely in english units, the latter exculsively in metric units. (See page 4 for definitions of variables.)

The equations used for the calculation of both the normalized resistance and reactance were adapted from Armstrong's work.[1:p. 21] Originally, these equations combined both english and metric units, however they were modified to work in uniform units.

The following are the equations used for normalized resistance in both ENGNOR and METNOR:

$$R/\rho c = RVDC + ZJ + \frac{\pi}{2\sqrt{2}} \frac{\sqrt{E}}{c} \exp(SN) \tag{1}$$

where in the english version (ENGNOR):

$$RVDC = \frac{.077t}{\frac{P_s}{14.6} OA} \frac{(T_t/519)^2}{(T_t/519 + .416)} \tag{2}$$

$$ZJ = \frac{.0000383(T_t/519)^{.75}\sqrt{f}\ (t/d + 1-OA)}{OA\sqrt{\frac{P_s}{14.7}\ (T_t/519 + .416)}} \tag{3}$$

$$E = 1.0251 \left(\frac{1}{(OA)^2} - 1\right) \left(\frac{1}{(OA)^{.1}}\right) \exp(-.5072t/d) \tag{4}$$

$$SN = -1.8(2.54df(OA)/V)^2 \tag{5}$$

The RMS total particle velocity is obtained using:

DEFINITIONS OF VARIABLES AND UNITS IN PERFORATED SHEET MODEL

Symbol	Definition	Units	
		English	Metric
c	speed of sound	ft/sec	m/sec
d	perforate hole diameter	in	cm
f	frequency	set^{-1}	sec^{-1}
L	panel core depth	in	cm
M	mach number	--	--
OA	percent perforate open area	decimal percent	
P_s	static pressure	PSI	N/m^2
t	thickness of perforated sheet	in	cm
T_t	total air temperature	°R	°K
V	RMS total particle velocity	ft/sec	cm/sec
V_{SPL}	RMS spectrum particle velccity	ft/sec	cm/sec
V_{GF}	RMS grazing flow particle velocity	ft/sec	cm/sec
θ	boundary layer momentum thickness	in	cm
ρ	local air density	lbm/ft^3	kg/m^3

$$V = \sqrt{V_{SPL}^2 + V_{GF}^2} \tag{6}$$

and the spectrum particle velocity is:

$$V_{SPL} = \frac{P_{RMS}(144q_c)}{\rho c} \tag{7}$$

where

$$P_{RMS} = 2.901 \times 10^{-9} \left(10^{\frac{SPL}{20}}\right)$$

The grazing flow contribution to velocity is:

$$V_{GF} = \frac{.25(XKK)cM^2}{\frac{RVDC}{2} + \sqrt{\frac{RVDC^2}{2} + \frac{XKK}{2} EM^2}} \tag{8}$$

where

$$XKK = \begin{cases} 0 & \text{if } \theta = 0 \\ .05 + .11(d/\theta) & \text{if } \theta \neq 0 \end{cases}$$

And for the metric version (METNOR):

$$RVDC = \frac{.030315t}{\frac{P_s}{101325} OA} \frac{(T_t/288)^2}{(T_t/288 + .416)} \tag{9}$$

$$ZJ = \frac{.0000383(T_t/288)^{.72}\sqrt{f}(T/d + 1 - OA)}{OA\sqrt{\frac{P_s}{101325}(T_t/288 + .416)}} \tag{10}$$

The equation for E is the same as equation (4)

$$SN = -1.8\left(df(OA)/V\right)^2 \tag{11}$$

$$V_{SPL} = \frac{P_{RMS}}{\rho c} \times 100$$

where

$$P_{RMS} = 2 \times 10^{-5} \left(10^{\frac{SPL}{20}}\right) \quad (12)$$

$$V_{GF} = (\text{Eqn. } 8) \times 100$$

The normalized reactance was calculated in ENGNOR using:

$$\frac{X}{\rho c} = \frac{.000469f}{OA\sqrt{T_t/519}} \{t + .85d(1-.7\sqrt{OA}) - (.0003657V/OA)\} - \cot(kL) \quad (13)$$

where

$$k = 2\pi f/12c$$

and in METNOR:

$$\frac{X}{\rho c} = \frac{.0001846f}{OA\sqrt{T_t/188}} \{t + .85d(1-.7\sqrt{OA}) - (.00003048V/OA)\} - \cot(kL) \quad (14)$$

where

$$k = 2\pi f/100c$$

Subroutines ENGHOL and METHOL were developed to solve the previous equations for the percent perforate open area (OA) and the panel core depth (L), when the normalized resistance and reactance are given quantities. ENGHOL is the english version, while METHOL is the metric version.

Due to the nature of the equations, the solutions for (OA) utilizes an iterative type algorithm. ENGHOL calls an internal subroutine LINPAR, obtained from Schauer, et. al.[3:p. 142] (LINPAT for METHOL), which determines an initial starting quantity for (OA), which is then used in the iterative scheme. The appropriate calculations are carried out, ($R/\rho c$) is calculated and compared to the input value, and if the difference is greater than .001, a new value is calculated. Once (OA) is determined, (L) is solved explicitly from equations (13) or (14), depending on the units used.

Polymide Sheet Impedance Model

The normalized resistance ($R/\rho c$) and normalized reactance ($X/\rho c$) can be calculated for a polymide sheet acoustic lining material, using Fortran IV Subroutines PIMENG and PIMMET. PIMENG uses only english units, while PIMMET is the metric version.

DEFINITIONS OF VARIABLES AND UNITS
IN POLYMIDE SHEET MODEL

Symbol	Definition	Units	
		English	Metric
c	speed of sound	ft/sec	m/sec
f	frequency	sec^{-1}	sec^{-1}
L	panel core depth	in	cm
M	mach number	--	--
T_s	static air temperature	°R	°K
V	RMS total particle velocity	ft/sec	cm/sec
V_{SPL}	RMS spectrum particle velocity	ft/sec	cm/sec
V_{GF}	RMS grazing flow particle velocity	ft/sec	cm/sec
ρ	local air density	lbm/ft^3	kg/m^3
N	number of plies (integer)	--	--

The equations used in the calculations were obtained and adapted from Armstrong.[1:p. 22]

The following are the equations used to obtain the normalized resistance in both PIMENG and PIMMET.

$$R/\rho c = (RVDC + S + T)/\rho c \tag{15}$$

where in PIMENG

$$RVDC = 460 \cdot A \cdot N^{1.333} \tag{16}$$

and

$$A = 1.115 \times 10^{-5} \left[\frac{T_s^{1.5}}{T_s + 216}\right]$$

$$S = .305 \cdot A \cdot N^2 \cdot f \tag{17}$$

$$T = 2.86 \rho N^2 V \tag{18}$$

The RMS total particle velocity is obtained using equation (6), and the RMS spectrum particle velocity is obtained from equation (7). The grazing flow contribution is obtained using

$$V_{GF} = \frac{.05cM^2}{\frac{RVDC}{\rho c} + \sqrt{\frac{RVDC^2}{\rho c} + .71N^2M^2}} \tag{19}$$

And in PIMMET

$$RVDC = 22650 \cdot A \cdot N^{1.333}$$

and

$$A = 1.496 \times 10^{-5} \left[\frac{T_s^{1.5}}{T_s + 120}\right] \tag{20}$$

$$S = 1.4891 \cdot A \cdot N^2 \cdot f \tag{21}$$

$$T = 2.86 \rho N^2 (V/100) \tag{22}$$

The RMS total particle velocity is obtained using equation (6) and the RMS spectrum particle velocity is obtained again using equation (12). The TMS grazing flow contribution is:

$$V_{GF} = \text{(Eqn. 19)} \times 100 \tag{23}$$

The normalized reactance is obtained in PIMENG using:

$$\frac{X}{\rho c} = [(.549\rho N^{1.5} f) - (5.12 \times 10^{-5} \rho N^3 fV)]/\rho c - \cot(kL) \quad (24)$$

where

$$k = 2\pi f/12c$$

and in PIMMET using:

$$\frac{X}{\rho c} = [(.1673\rho N^{1.5} f) - (5.12 \times 10^{-5} \rho N^3 fV)]/\rho c - \cot(kL) \quad (25)$$

where

$$k = 2\pi f/100c$$

Subroutines LINENG and LINMET were developed to solve the previous equations for the number of plies (N) and the panel core depth (L), when the normalized resistance and reactance are given quantities. LINENG is the english version while LINMET is the metric version.

Because of the nature of equation (15), the number of plies required to obtain a given resistance cannot be solved for explicitly. Therefore (N) is initially given a value of 1.0, then equation (15) is solved. The answer is compared to the input value, and if the difference was greater than .001, the value of N was modified accordingly. Once N is determined, (L) is solved for explicitly in LINENG using equation (24) or in LINMET using equation (25).

In summary, for perforated plate or polymide sheet duct linings the relationships between the physical dimensions and the acoustical properties have been programmed. The program gives either the acoustical properties when the physical dimensions are input or vice versa. The programming is required because of complexity of the relationships and because an iterative solution is necessary when going from the acoustical properties to the physical dimensions. The details of the program are given in the program users manual.

SECTION III

AXIAL PROPAGATION CONSTANT ESTIMATION

For a cylindrical duct with no flow we would like to estimate the axial propagation constant, $\tau - i\sigma$, for a given angular and radial mode number (m,n) and for a given wall impedance, $R + iX$. The technique is to estimate τ, the phase velocity, for the desired mode by assuming a hard wall. Then to estimate σ, the duct attenuation, based on ray acoustics as given by Rice, et al [2].

From the governing partial differential equations a separation of variables gives a solution in terms of Bessel functions in the radial direction. The phase velocity for a hard wall is related simply to the zero's of the derivative of the Bessel function. These zero's are real for a hard wall and as can be seen from Rice, et al [2] equation 7 for no flow,

$$\tau_{mn} = \sqrt{1 - \left(\frac{\alpha_n}{\pi\eta}\right)^2} \tag{26}$$

where

τ_{mn} is the phase velocity of the m^{th} angular, n^{th} radial mode

η is the frequency parameter, $\eta = fD/c$, the frequency times the duct diameter over the speed of sound

and

α_n is the n^{th} zero of $J_m'(\alpha_n) = 0$, J_m being the m^{th} order Bessel function.

This relationship also permits identification of cutoff modes, the mode which does not propagate in the hard duct, as the modes having α_n's large enough to make the phase velocity τ imaginary. The radial propagation angle, ϕ_r, defined by Rice to be the angle of incidence of the wave front on the wall is given by Rice and Heidman [4], equation 19 evaluated at the wall for real α_n as:

$$\cos \phi_r = \frac{1}{\pi\eta} \sqrt{\alpha_n^2 - m^2} \tag{27}$$

The axial propagation angle, defined by Rice, et al to be the angle the wave front makes with the centerline can be evaluated by equation 5 of Reference 2 as:

$$\cos \phi_x = \tau_{mn}$$

Then, consideration of a wave incident on the wall and reflected back with the angle of incidence equal to the angle of reflection and meeting the soft wall boundary condition gives for the ratio of axial energy flux after the bounce to that before as equation 25 of Reference 2:

$$\frac{I_x^-}{I_x^+} = \frac{(R^2 + X^2) \cos^2 \phi_r - 2R \cos \phi_r + 1}{(R^2 + X^2) \cos^2 \phi_r + 2R \cos \phi_r + 1} \tag{28}$$

For N bounces the attenuation constant σ may be estimated as:

$$\sigma = \frac{10N}{27.3\eta} \log_{10} \frac{I_x^-}{I_x^+} \tag{29}$$

The number of bounces, N, is not clear because of the variation of σ_r with r in the duct, but matching the estimated value of σ with the exact value for some typical cases shows that:

$$N = \frac{1}{2} \tan \phi_r = \frac{\frac{1}{2} \alpha_n / \pi\eta}{\sqrt{1 - (\alpha_n/\pi\eta)^2}} \tag{30}$$

gives reasonable agreement. Equation 29 then permits the attenuation constant σ to be estimated in a simple direct way. The exact technique must use an iterative process, with an initial guess required for τ and σ. Use of these estimates as the initial guess usually permits the exact technique to converge to the desired mode.

These relationships were programmed to permit their repeated evaluation for all propagating modes. The details of the program are in the Users Manual for Suppressor Performance Estimation included as part of this report. The Users Manual compares the estimates to the exact values and shows that the estimates are poor when the radial propagation angle is close to zero or $\pi/2$ radians. This is to be expected since these angles correspond to no bounce or infinitely many bounces as the wave propagates down the duct. Infinitely many bounces occur as cutoff is approached. Zero bounces corresponds to the hard wall propagation of a plane wave. For most of the higher order modes which are not too close to cutoff, however, the procedure gives useful results.

SECTION IV

SHEARED FLOW ORTHOGONALITY

INTRODUCTION

An orthogonal condition which permitted isolation of the modal coefficients for an expansion of an arbitrary initial pressure distribution in terms of the sheared flow pressure modes was investigated in an Aero Propulsion Laboratory report [3]. In addition to a satisfactory solution of the adjoint problem for the second order partial differential equation, it was recognized that the second order equation did not permit an arbitrary initial velocity both axially and radially, as is physically possible. This led to the effort reported here, which includes investigations in several areas. Hydrodynamic modes were investigated in uniform flow and sheared flow. Because of difficulty with the sheared flow hydrodynamic modes, a simple linear velocity profile flow with a small Mach number was studied. The perturbation approach used did not result in a solution which satisfied all the boundary conditions.

HYDRODYNAMIC MODES IN UNIFORM FLOW

For a rectangular duct with uniform flow M in the axial, or x direction the continuity, x and y momentum equations for the perturbations are respectively:

$$u_x + v_y = -\frac{1}{\rho c^2}\,[P_t + cMP_x]$$

$$u_t + cMu_x = -\frac{1}{\rho}\,P_x \qquad (31)$$

$$v_t + cMv_x = -\frac{1}{\rho}\,P_y$$

where u and v are the axial and cross duct velocities and c is the speed of sound. Here ρ is the mean density. For sinusoidal motion in time u, v, and P are proportional to $\exp(i\omega t)$ and for $k = \omega/c$ we get:

$$u_x + v_u = = \frac{1}{\rho c}\,(ikP + MP_x)$$

$$iku + Mu_x = -\frac{1}{\rho c}\,P_x \qquad (32)$$

$$ikv + Mv_x = -\frac{1}{\rho c}\,P_y$$

Looking for a hydrodynamic solution which has no fluctuating pressure associated with it would mean setting P, P_x, P_y equal to zero in Equation 32 leaving

$$u_x + v_y = 0, \qquad iku + Mu_x = 0, \qquad ikv + Mu_x = 0 \tag{33}$$

multiplying the momentum equations (Equation 33) by dx and integrating while holding y constant gives:

$$u = e^{-\frac{ik}{M}x} \cdot f(y) \quad \text{and} \quad v = e^{-\frac{ik}{M}x} \cdot g(y) \tag{34}$$

where f and g are arbitrary functions of y except that the boundary condition on v at the duct walls is that v must be zero in order to avoid effecting the acoustical wall impedance. To meet this boundary condition on v at y = 0 and at y = 1, g(y) can be built up by

$$v = e^{-\frac{ik}{M}x} \sum_{n=1}^{\infty} a_n \sin n\pi y \tag{35}$$

Substituting Equation (35) into the continuity equation of Equation (33) gives:

$$u = e^{-\frac{ik}{M}x} \sum_{n=1}^{\infty} b_n \sin n\pi y \tag{36}$$

where a_n and b_n must be related by:

$$a_n = \frac{ik}{n\pi M} b_n \tag{37}$$

Further, taking $(\ )_x$ of the y momentum equation and $(\ )_y$ of the x momentum equation of Equation (33), subtracting and solving the resultant equation as before gives the fluctuating vorticity as

$$v_x - u_y = e^{-\frac{ik}{M}} h(y) \tag{38}$$

where h(y) is related to f and g such that:

$$h(y) = \sum_{n=1}^{\infty} \left[\left(\frac{k}{M}\right)^2 + (n\pi)^2\right] \frac{b_n}{n\pi} \sin n\pi y \tag{39}$$

The fluctuating vorticity then travels down the duct in cells of length Mc/f, where f is the frequency and moving at the speed of the flow, Mc, as can be seen by putting the time dependence back in, giving u, v, and $v_x - u_y$ all proportional to

$\exp(-ik/M(x-Mct))$. These fluctuating velocities without fluctuating pressures are called the hydrodynamic modes.

A similar solution can be found in axisymmetric uniform mean flow situations.

SHEARED FLOW STUDY

For a rectangular duct with a sheared flow where M is a function of y only, the continuity, x and y momentum equations with sinusoidal time dependence for the perturbations are respectively:

$$u_x + v_y = -\frac{1}{\rho c}(ikP + MP_x)$$

$$iku + Mu_x + vM' = -\frac{1}{\rho c} P_x \qquad (40)$$

$$ikv + Mv_x = -\frac{1}{\rho c} P_y$$

These differ from the uniform flow equations (Equation 32) only by the addition of a single term in the x momentum equation. Although this seems to be only a small difference, it causes a coupling between the fluctuating velocity field and the fluctuating pressure field. While the irrotational mean flow equations (Equation 32) can be reduced to a second order equation in pressure alone these sheared flow equations reduce to a third order partial differential equation in pressure alone.

Although considerable effort was expended in an effort to find solutions to the set of equations (Equation 40), no solutions matching duct boundary conditions were found. Among the techniques tried were perturbation-type solutions for $M = M_0 + \varepsilon y$, where ε is a small parameter.

SECTION V

VARIABLE AREA DUCTS

INTRODUCTION

Because aircraft ducts have a variable cross-sectional area, the sound propagation in such ducts is of interest. The complexity of the governing partial differential equation and boundary conditions for fluctuating pressures and velocities under these conditions has led to numerical methods as the appropriate technique for solving these governing equations. A November 1980 survey of numerical techniques by Baumeister [5] shows the progress in this area and the current limitations. This effort is in good agreement with Baumeister's comments that transient numerical techniques which step the governing equations ahead in time are very promising. The present effort combines these transient techniques as detailed by Baumeister in References 6 and 7 with mapping techniques introduced by Quinn [8]. Quinn's analytical maps for particular duct shapes are extended here to a numerical mapping technique for general duct shapes including bullet nose type aircraft inlets. The mapping technique consists of a coordinate transformation which maps the duct boundaries into a rectangle. The governing partial differential equations are transformed by this coordinate change into a new set of partial differential equations which may be solved together with the transformed boundary conditions in the rectangle using finite-difference methods.

Two programs were developed. The first program called TDEP solved the no flow problem in a variable area duct for arbitrary wall impedance distribution. The second program, called TDEPF, solved the governing equations with flow for an axisymmetric potential flow distribution. This irrotational flow gives no coupling between the pressure distribution and hydrodynamic modes.

NO FLOW VARIABLE AREA DUCT ACOUSTICS

The asixymmetric no flow governing partial differential equations can be reduced to:

$$P_{zz} + P_{rr} + \frac{1}{r} P_r + \frac{1}{r^2} P_{\theta\theta} = \eta_r^2 P_{tt} \qquad (41)$$

as given for example by Baumeister [7]. Here r, z, and θ are the usual cylindrical coordinates with lengths nondimensionalized by dividing by R, P is the fluctuating pressure nondimensionalized by ρc^2 and $\eta_r = Rf/c$, the initial duct radius or

annular radius difference times the frequency f, divided by the acoustic velocity c. The mean density ρ is used in making P dimensionless. Time is also made dimensionless here by $t = f \cdot \text{time}$.

The θ variation is assumed to be proportional to $e^{im\theta}$ giving $P_{\theta\theta} = -m^2 P$. Equation (41) then is reduced to two space variables. Following Quinn [8] we define a coordinate transformation $z = f(x,y)$, $r = g(x,y)$. Then for a conformal coordinate transformation satisfying the Cauchy-Riemann conditions $f_x = g_y$ and $f_y = -g_x$ Equation (16) transforms to:

$$P_{xx}+P_{yy} + \frac{f_x}{g} P_y - \frac{f_y}{g} P_x - \frac{m^2}{g^2} (f_x^2+f_y^2)P = (f_x^2+f_y^2)\eta^2 P_{tt} \quad (42)$$

The boundary conditions on a soft wall $\zeta = P/V'$, where ζ is the wall impedance over ρc and V' is the normal component of velocity, are substituded into the normal momentum equation:

$$V'_t = - \frac{1}{\eta} P_N \quad (43)$$

to give

$$P_N = - \frac{\eta}{\zeta} P_t \quad (44)$$

as the boundary condition in the duct. This transforms to:

$$P_y = - \frac{\eta (f_x^2+f_y^2)^{1/2}}{\zeta} P_t \quad (45)$$

for the outer soft wall boundary condition.

In a similar manner the exit impedance ζ_e appears in the duct exit boundary condition as:

$$P_x = - \frac{\eta (f_x^2+f_y^2)^{1/2}}{\zeta_e} P_t \quad (46)$$

The exit impedance was taken from Baumeister [7] to be $\zeta_e = [1 = (\alpha_{mn}/2\pi\eta_r)^2]^{1/2}$.

The inner wall of annular sections was taken as hard but it could easily satisfy a soft boundary condition Equation (45) with the sign on P_y changed to negative. On the centerline of cylindrical ducts the conditions applied were $P_y = 0$ for angular mode $m = 0$ or $P = 0$ for $m \geq 1$.

The entrance condition used follows Baumeister [7]:

$$P(o,y,t) = J_m(\alpha_{mn}y)e^{2\pi it} \tag{47}$$

where J_m and α_{mn} were as in Equation (26)

The initial condition in the duct was

$$P(x,y,o) = 0; \qquad P_t(x,y,o) = 0 \tag{48}$$

The finite difference representation of Equation (42) and its boundary conditions was based on central differences, again following Baumeister [7]. Table 1 shows the coefficients in:

$$P^{k+1}_{i,j} = 2P^{k}_{i,j} - P^{k-1}_{i,j} + \frac{(\Delta t)^2}{\eta^2(\Delta y)^2(f_x^2+f_y^2)}\,\psi_\ell \tag{49}$$

where

$$\psi_\ell = A_\ell P^{k}_{i-1,j} + B_\ell P^{k}_{i,j-1} + C_\ell P^{k}_{i,j} + D_\ell P^{k}_{i+1,j} + E_\ell P^{k}_{i+1,j} + F_\ell P^{k+1}_{i,j} + G_\ell P^{k-1}_{i,j} \tag{50}$$

and the ℓ subscript denotes the cell location. Cell 1 is an interior cell, cell 2 on the outer boundary, cell 3 on the inner boundary or centerline, cell 4 in the exit plane, cell 5 the outer boundary exit plane corner cell, and cell 6 the inner boundary exit plane corner cell.

As seen from Table 1 the coefficients in Equation (50) depend on the partial derivatives of the mapping function $z = f(x,y)$ and on g from $r = g(x,y)$. These were obtained from the conformal mapping technique as detailed under the subheading "Duct Mapping".

The steady-state pressures were evaluated from $P(x,y) = P(x,y,t)/\exp(2\pi it)$. Stability of the system was greatly improved by adding damping with:

$$P^{k+1} = P^{k+1} + DD\,[P^{k-1}e^{4\,i\,t} - P^{k+1}] \tag{51}$$

at each grid point after a pass to compute new pressures. Here DD is the damping factor with no effect for DD = 0 and no change in the steady-state solution for DD = 1. A DD of 0.2 seemed to damp oscillations well without changing the steady-state solution. The addition of this damping seemed to permit soft walled solutions to be stable with a hard walled initial pressure mode at the duct entrance.

TABLE 1

COEFFICIENTS IN DIFFERENCE EQUATIONS

Cell Index	Difference Elements						
	A_ℓ	B_ℓ	C_ℓ	D_ℓ	E_ℓ	F_ℓ	G_ℓ
1	$\left(\frac{\Delta y}{\Delta x}\right)^2 + \frac{fy}{2g}\,\frac{(\Delta y)^2}{\Delta x}$	$1 - \frac{f_x \Delta y}{2g}$	$-2\left[1 + \left(\frac{\Delta y}{\Delta x}\right)^2\right] - \frac{(\Delta y)^2 m^2 (F2)}{g^2}$	$1 + \frac{f_x \Delta y}{2g}$	$\left(\frac{\Delta y}{\Delta x}\right)^2 - \frac{f_y (\Delta y)^2}{2g\Delta x}$	0	0
2	A_1	2	C_1	0	E_1	$-\frac{\Delta y}{\Delta t}\,\frac{\eta}{\zeta}(F2)^{1/2} - \frac{f_x}{2g}\,\frac{\eta}{\zeta}\frac{(\Delta y)^2}{\Delta t}\,(F2)^{1/2}$	$-F_2$
3	A_1	0	C_1	2	E_1	0	0
4	$2\left(\frac{\Delta y}{\Delta x}\right)^2$	B_1	C_1	D_1	0	$\frac{(\Delta y)^2}{\Delta t}\,\frac{\eta}{\zeta_e}(F2)^{1/2} - \left(\frac{fy}{2q} - \frac{1}{\Delta x}\right)$	$-F_4$
5	A_4	2	C_1	0	0	$F_2 + F_4$	$-F_5$
6	A_4	0	C_1	2	0	F_4	$-F_4$

$$F2 = f_x^2 + f_y^2$$

Baumeister's straight duct no-flow results of Reference 7 for the third angular mode were duplicated. Quinn's analytical conical duct solution was compared to the TDEP solution for the zero angular mode giving a good comparison with damping introduced. Quinn's hard wall hyperbolic horn for the third angular mode was also run as a test case for the acoustic transient technique. The zero angular mode in a soft walled straight duct approached the same steady solution with several different values of damping introduced. Several variable area duct configurations were run satisfactorily. The bullet nose inlet configuration is shown in Figure 1. The resultant pressure distribution along the bullet nose duct outer wall surface for a plane wave is shown in Figure 2. These results are for a dimensionless wall impedance $\zeta = 9 - i$ on the outer wall with the inlet bullet hard.

INCOMPRESSIBLE FLOW VARIABLE AREA DUCT ACOUSTICS

Writing all the variables in dimensionless form using the initial duct radius, R, the sound frequency, f, the speed of sound, c, and the mean density, ρ, gives $r = r^*/R$, $z = z^*/R$, $t = ft^*$, $P = P^*/c$, $u = u^*/c$, $v = v^*/c$, $w = w^*/c$, $U = U^*/c$, $V = V^*/c$, $W = W^*/c$. Here the stared variables refer to the dimensional quantities. With $\eta = Rf/c$ the following set of partial differential equations governs the fluctuating variables:

$$\eta P_t + v_r + u_z + \frac{v}{r} + \frac{imw}{r} + (V_r + U_z + \frac{V}{r})P + VP_r + UP_z = 0$$

$$\eta u_r + Vu_r + Uu_z + vU_r + uU_z + (VU_r + UU_z)P = -P_z$$

$$\eta v_t + Uv_z + Vv_r + uV_z + vV_r + (VV_r + UV_z)P = -P_r \qquad (52)$$

$$w_t + Uw_z + Vw_r + \frac{V}{r}w = -im\frac{P}{r}$$

These equations representing continuity and the three momentum equations are analogous to those given by Quinn [9] and Eversman, et al [10]. In the last equation of the set (Equation (52) the assumption that P is proportional to $\exp(im\theta)$ has again been incorporated. With our coordinate transformation $z = f(x,y)$, $r = g(x,y)$ satisfying the Cauchy-Riemann conditions, Equations (52) transform to:

$$f_2\eta P_t - f_y v_x + f_x v_y + f_x u_x + f_y u_y + f_2(v + imw)/g$$

$$+ P(-f_y V_x + f_x V_y + f_x U_x + f_u U_y + f_2 V/g)$$

$$+ (f_x U - f_y V)P_x + (f_y U + f_x V)P_y = 0$$

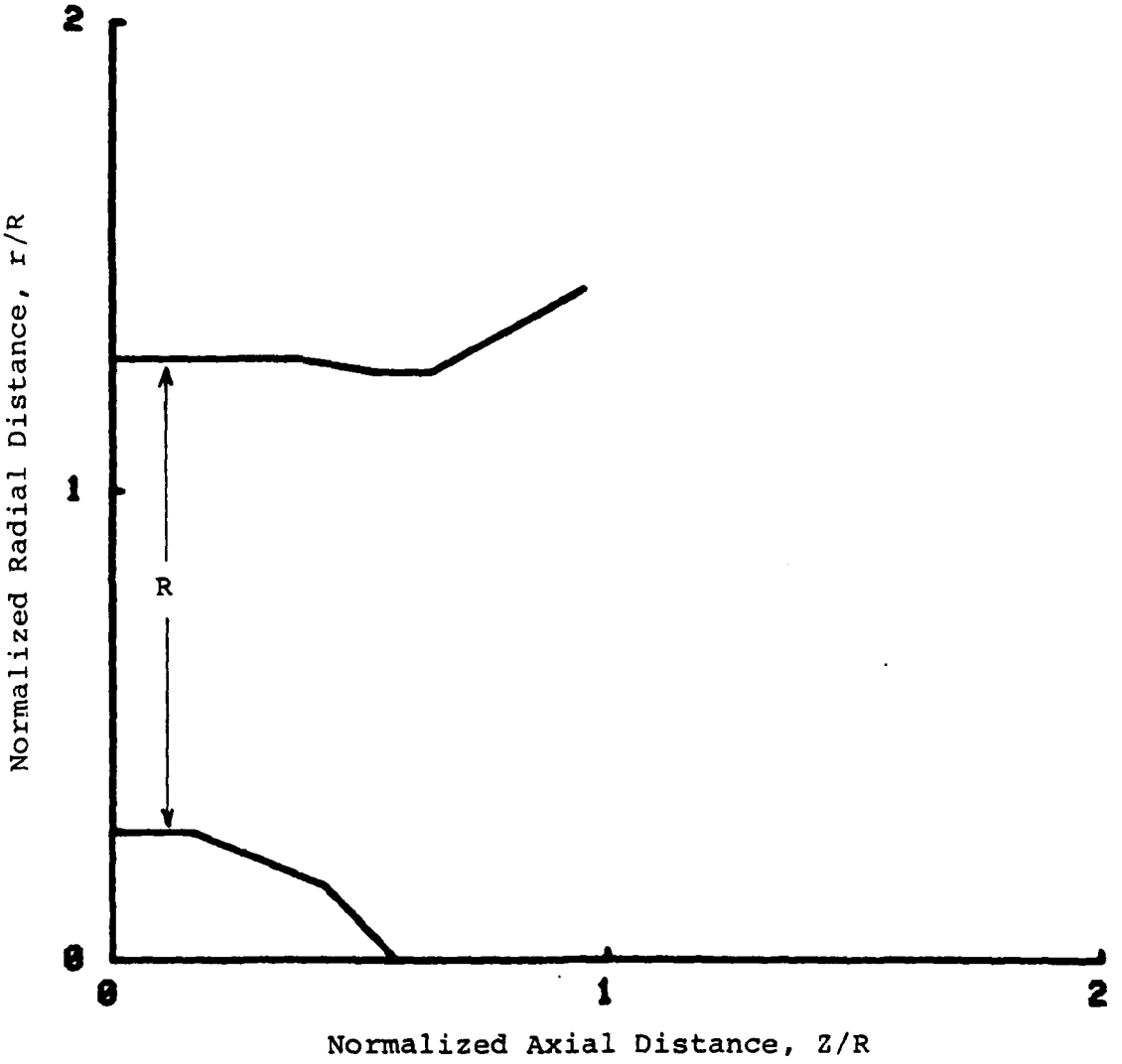

Figure 1. Bullet Nose Duct Profile

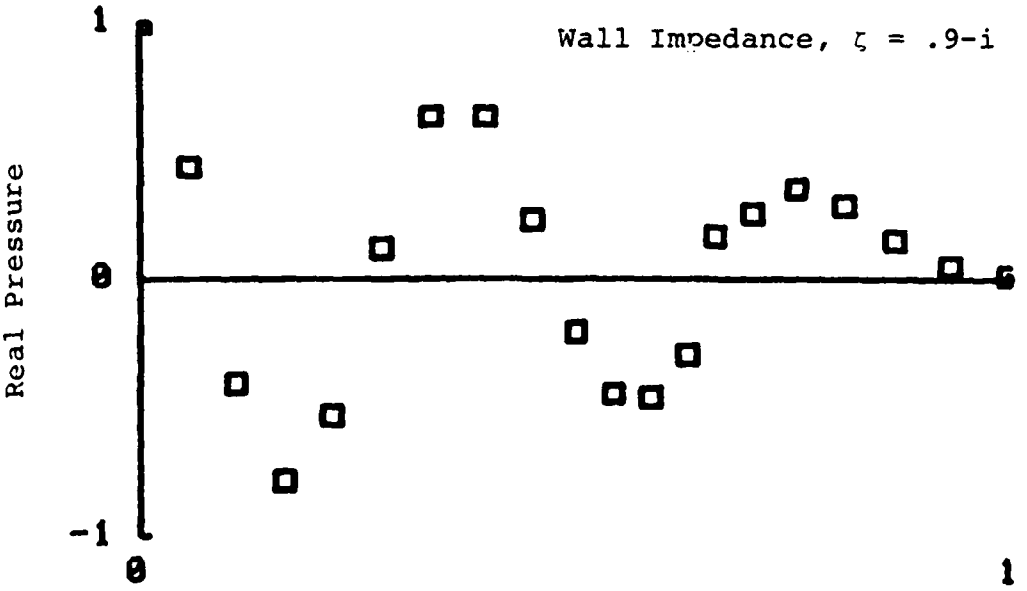

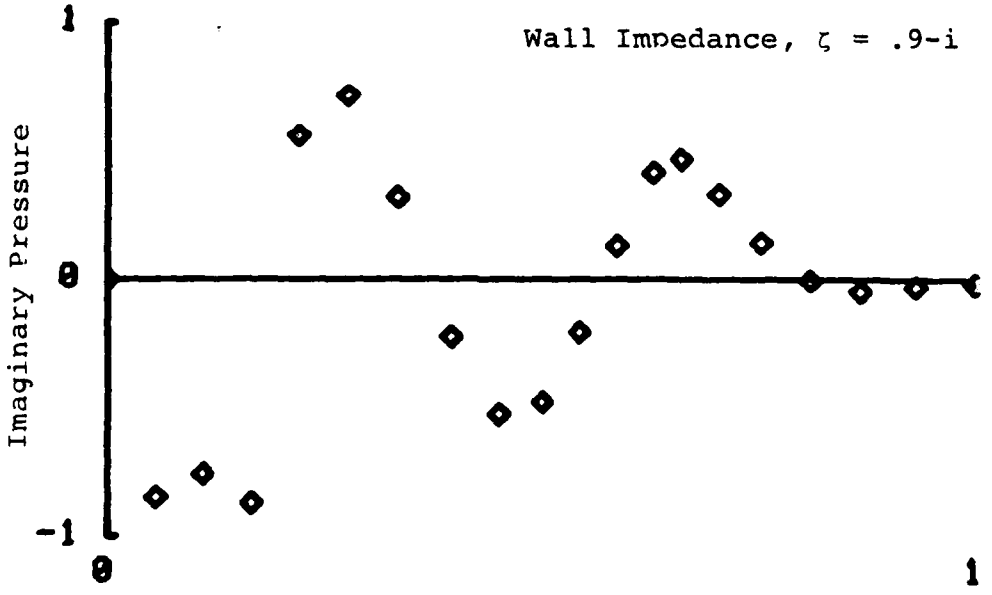

Figure 2. Pressure Distribution in Bullet Nose Inlet

$$f_2\eta u_t + (f_x U - f_y V)u_x + (f_y U + f_x V)u_y$$
$$+ (f_x u - f_y v + f_x PU - f_y PV)U_x$$
$$+ (f_y u + f_x v + f_y PU + f_x PV)U_y + f_x P_x + f_y P_y = 0$$

$$f_2\eta v_t + (f_x U - f_y V)v_x + (f_y U + f_x V)v_y$$
$$+ (f_x u - f_y v + f_x PU - f_y PV)V_x$$
$$+ (f_y u + f_x v + f_y PU + f_x PV)V_y - f_y P_x + f_x P_y = 0$$

$$f_2\eta w_t = (f_x U - f_y V)w_x + (f_y U + f_x V)w_y + f_2(w + imP)/g = 0$$

(53)

where $f_2 = f_x^2 + f_y^2$.

The boundary conditions on the soft outer wall of the duct should be:

$$v_t' = P_t/\zeta + U'(P/\zeta)_\tau/\eta \qquad (54)$$

where v' is the normal velocity component, U' is the mean tangential velocity component and τ denotes the tangential direction.

Because of stability problems the boundary condition used was simply:

$$P = \zeta V' \qquad (55)$$

with u, v and w computed from the momentum equation, the bottom three equations in Equation (53).

On the inner wall or centerline the boundary conditions used were:

$$P_N = 0 \quad \text{and } v' = 0, \quad w = 0 \qquad (56)$$

where P_N is the normal derivative of pressure and the z direction velocity, u, is computed from the z momentum equation, the second equation in Equation (53).

The inlet boundary condition was taken as:

$$P = J_m(\alpha_{mn} y)\exp(2\pi i t) \tag{57}$$

where α_{mn} was the radial engenvalue for a cylindrical duct with the inlet cross-section. The variables u, v and w were computed from the momentum equations of Equation (53) at the inlet.

The exit plane was computed from $P = \zeta_e u_N$ where u_N is the normal velocity component and ζ_e is taken from Baumiester [7] as:

$$\zeta_e = (1 - M\beta)/(\beta - M) \tag{58}$$

where

$$\beta = \{[1 - (\alpha_{mn}/2\pi\eta)^2](1 - M^2)\} \tag{59}$$

Again u, v and w were computed from the momentum equation in Equation (53).

The initial condition in the duct was taken as P=u=v=w=0 or, in some computer runs, the steady solution was estimated and used as an initial condition to reduce run time.

The finite difference representation of Equation (53) and the boundary conditions was based on a predictor-corrector MacCormack method with generalization as suggested by Petty [11] to cause truncation errors in both to be proportional to the space difference squared (second order accurate). The top equation of Equation (53), the fluctuating continuity equation was written:

$$p_{ij}^{\overline{k+1}} = p_{ij}^{k} - (\Delta t/\eta f_2)\,(\text{space derivatives in } v,u,w,U,V, \text{ and } P) \tag{60}$$

for a predictor and

$$p_{ij}^{k+1} = (p_{ij}^{k} + p_{ij}^{\overline{k+1}})/2 \; - (\Delta t/2\eta f_2)\,(\text{same space derivatives}) \tag{61}$$

as a corrector. The space derivatives specified by Equation (53) were evaluated in the predictor using a forward difference at interior points and where it was feasible on the boundary. At boundary points where forward differences were not feasible backward differences were used. In the corrector the space derivatives were evaluated by a subroutine which used backward differences at interior points and three point formulations as developed by Petty [11] to maintain the second order accuracy at the boundary points.

The time and space derivatives were handled in an analogous manner for the time derivatives of u, v and w in the fluctuating z, r and θ momentum equations respectively of Equation (53).

Where boundary conditions were specified in Equations (54) through (58) the appropriate equation from Equation (53) was replaced by the boundary condition equation and the other three quantities were stepped forward in time using the remaining three equations of Equation (53).

Some difficulty was experienced in obtaining stable solutions of this set of equations and boundary conditions. Damping the solution by equations of the form in Equation (51) did not help stablize the solution. Different combinations of boundary conditions were tried but no formulation was found which produced stable results over the entire range of parameters desired. The solution seemed sensitive to the specification of the boundary conditions. The formulation specified produced good solutions for a slightly flared duct at Mach numbers of -.2 to +.1 as shown in Figure 3.

DUCT MAPPING

The variable area duct acoustics problem was solved by mapping the interior of the duct in terms of z and r into the interior of a rectangular region specified by x and y. The mapping used was based on the conformal Schwartz-Christoffel transformation as presented in Reddick and Miller [12] (page 423). Following the standard technique the duct shown in Figure 1 was mapped via:

$$\frac{dw}{dF} = K(e^{\pi F}-a_1)^{\alpha_1/\pi-1}(e^{\pi F}-a_2)^{\alpha_2/\pi-1}\cdots(e^{\pi F}-a_6)^{\alpha_6/\pi-1} \qquad (62)$$

Here $w = z + ir$ and $F = x + iy$. The real constants a_i are interpreted as vertex locations on the real axis in an intermediate plane, the Z plane where $Z = \exp(\pi F)$. The duct was

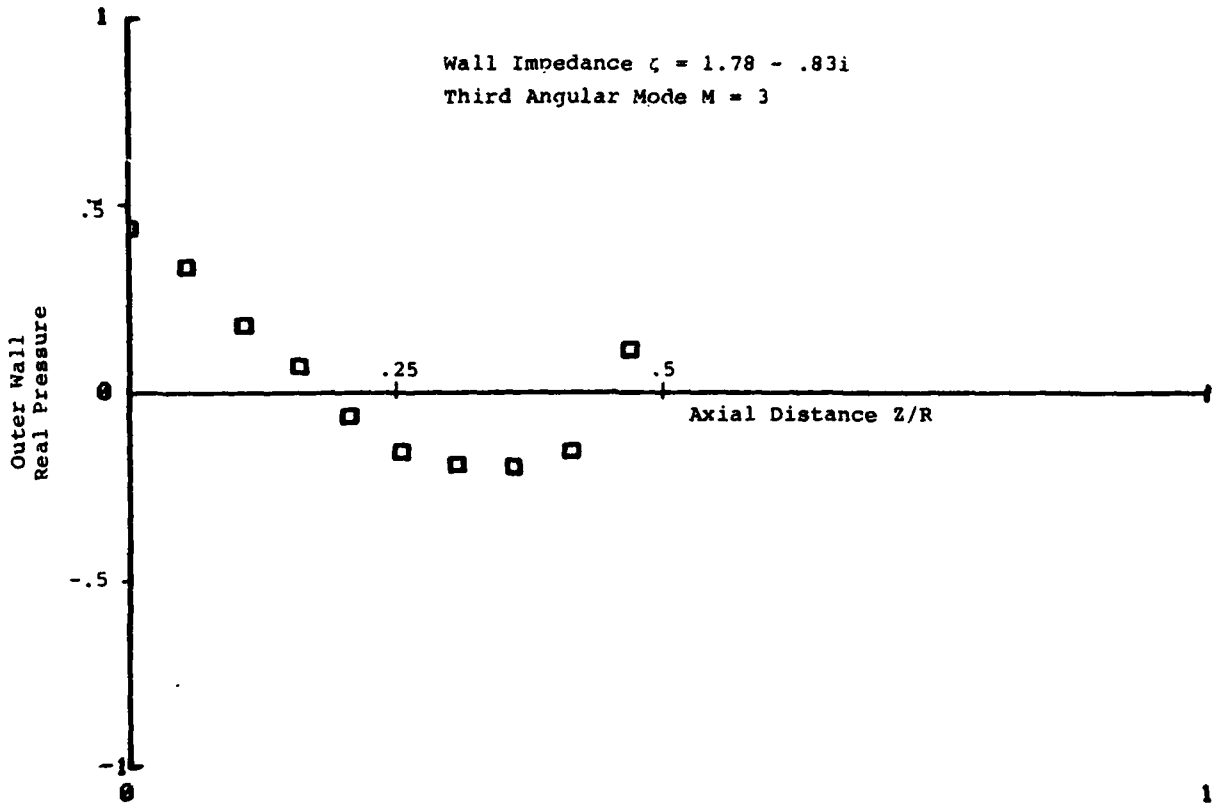

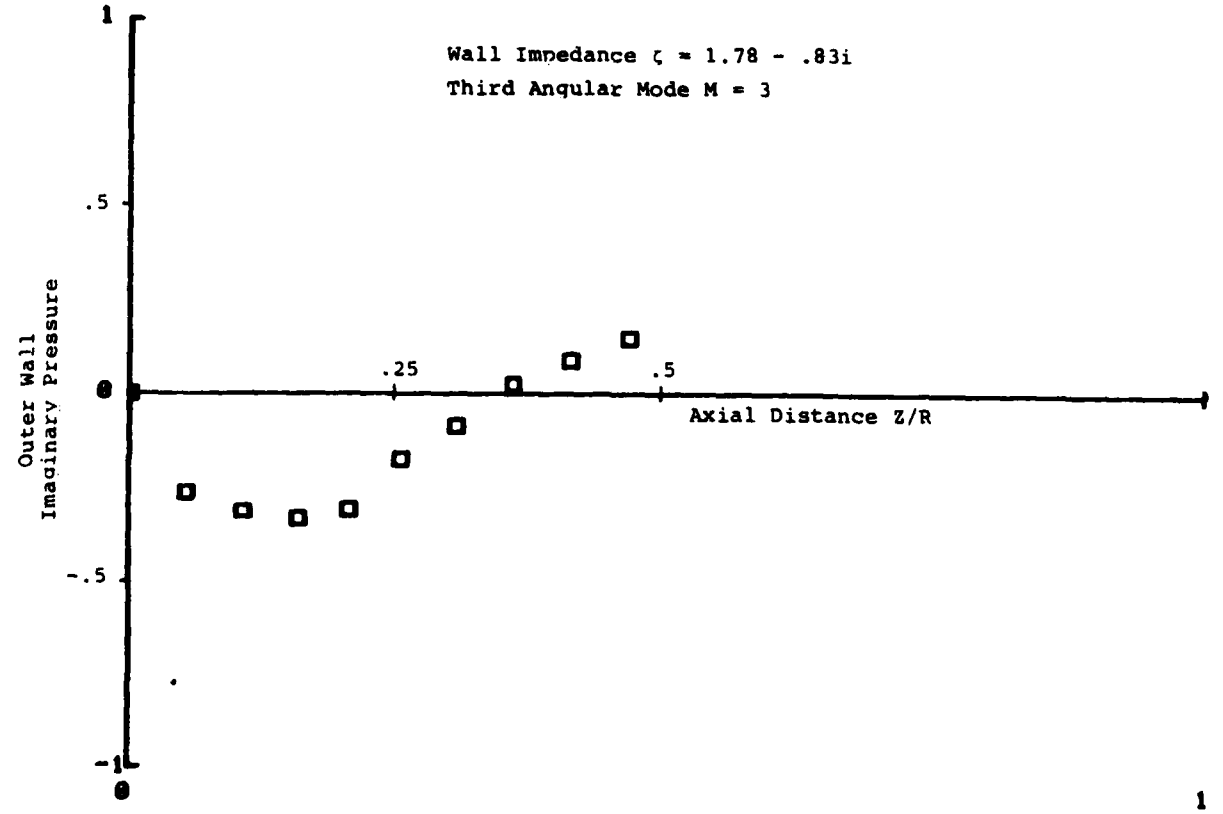

Figure 3a. Soft Flared Duct - Mach No. = -.2

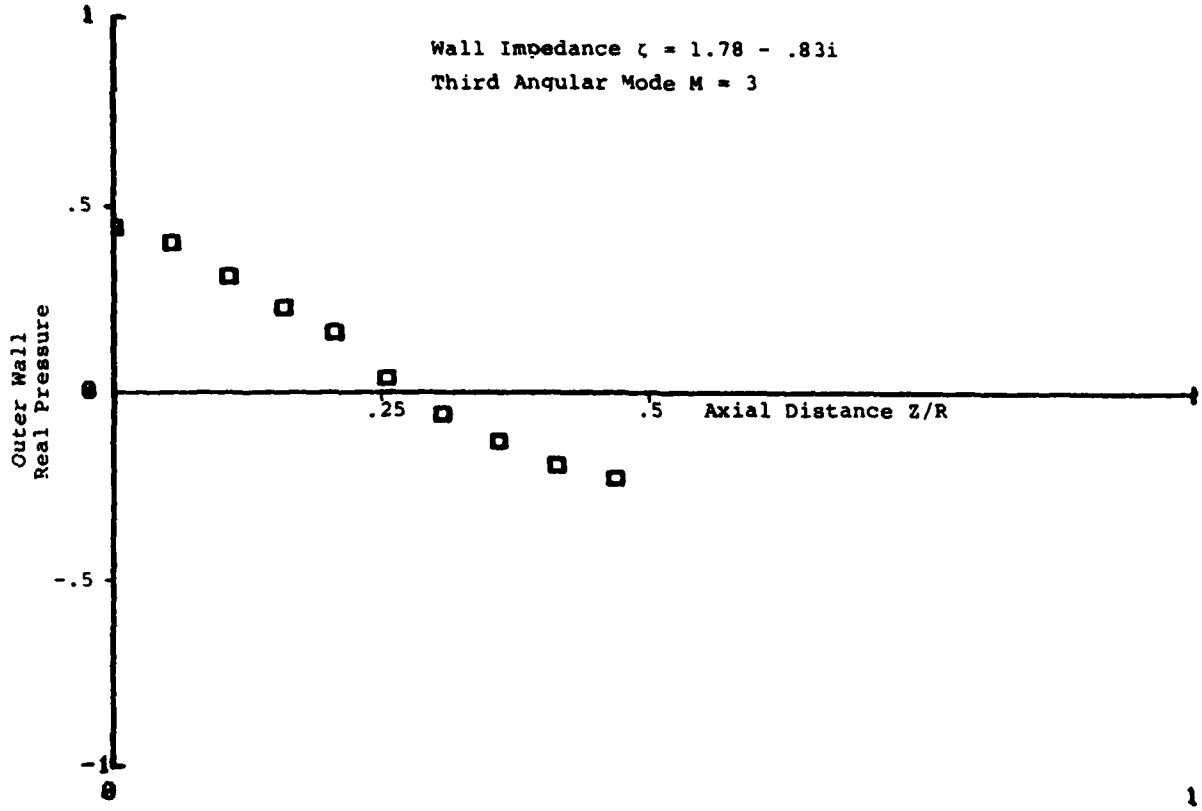

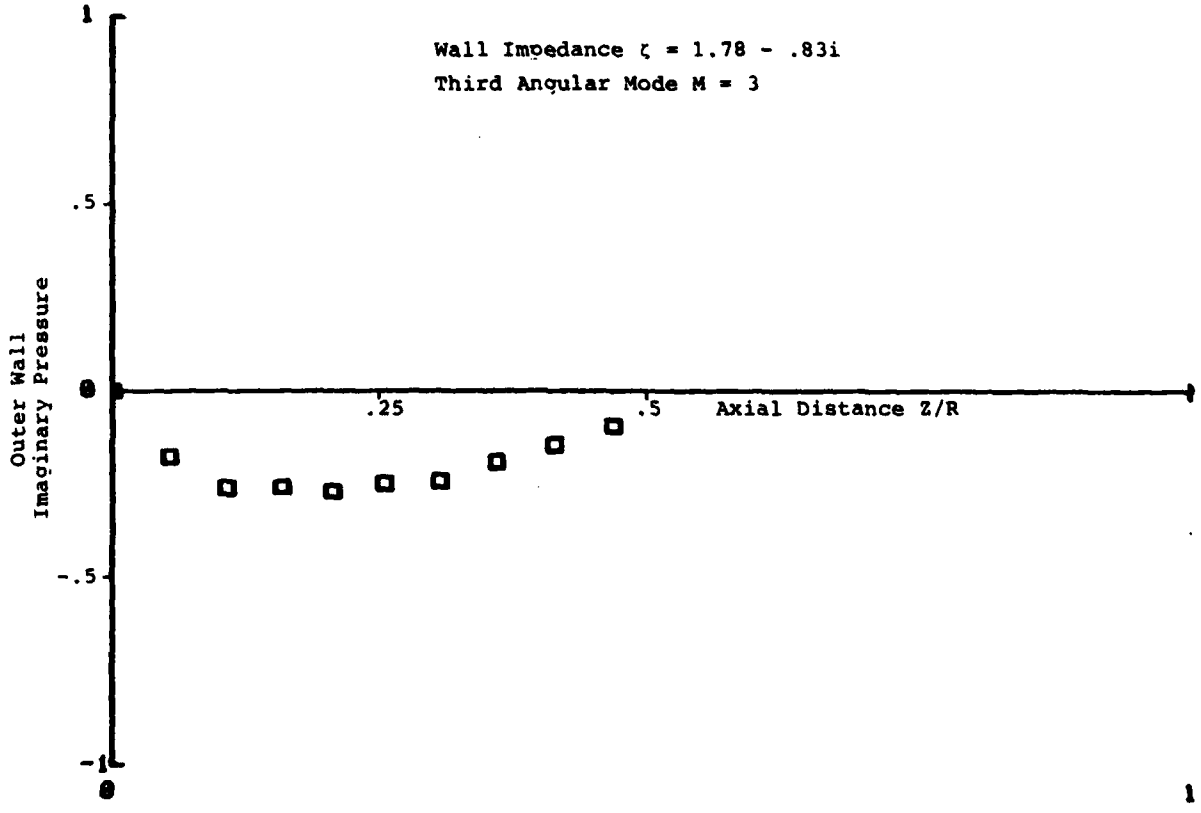

Figure 3b. Soft Flared Duct - Mach No. = .1

assumed to have zero included angle between the sides at the inlet and differential in radius of 1 at the inlet. That is, Δw at Z = 0 or F of minus infinity is i. Expressing w in exponential form and comparing the change in w equal i for Z going from R exp(0) to R exp(πi) as R approaches zero gives K as:

$$K = 1/\pi \cdot (-a_1)^{\alpha_1/\pi - 1} \cdot (-a_2)^{\alpha_2/\pi - 1} \cdots (-a_6)^{\alpha_6/\pi - 1} \tag{63}$$

The negative values of a_i corresponding to the outside wall are straightforward in Equation (63) and the positive values corresponding to the inner wall which result in a negative value to a power are evaluated from:

$$(-a_i)^{\beta_i} = [|a_i| \cdot \exp(\pi i)]^{\beta_i} = |a_i|^{\beta_i} \exp(\pi i \beta_i) \tag{64}$$

In order to use the mapping, the radius at a given value of x and y must be found because it appears directly in the governing partial differential equations. The values of w = z + ir are found from the integration:

$$w = \int \frac{dw}{dF}\, dF = \int \frac{dw}{dF}\, d(x + iy) \tag{65}$$

or

$$w = \int \frac{dw}{dF}\, dx + i \frac{dw}{dF}\, dv \tag{66}$$

For the dw/dF used (Equation 62) this integral is of the form:

$$w = \int P dx + Q dy \tag{67}$$

with $\partial P/\partial y = \partial Q/\partial x$ except on y = 0. Reddick and Miller [12] (page 441) shows that Green's lemma implies that the integral of Equation (65) is independent of path for these conditions as long as all paths are above the singularities on y = 0. A numerical integration in the F plane was used to evaluate w = z + ir at all grid points. The integration was carried out by integrating horizontally along the j = 4 set of grid points and then integrating vertically for the various i values.

With the conformal mapping established it can be shown that:

$$(\ )_z = [f_x(\ )_x + f_y(\ )_y]/(f_x^2 + f_y^2) \tag{68}$$

and

$$(\ )_r = [f_x(\ )_y - f_y(\ )_x]/(f_x^2 + f_y^2)$$

These relationships permit transformation of the governing partial differential equations (Equation 41 or 52) and their corresponding boundary conditions.

SECTION VI

NOISE/PERFORMANCE MODEL INTEGRATION

LEAST ATTENUATED MODE INTEGRATION

Previous contractual efforts had produced a theory for the maximum attenuation of the mode attenuated least in rectangular, annular, and cylindrical ducts. This theory was for constant area ducts with flows at Mach numbers of magnitude less than 0.5 and boundary layer thicknesses less than seven percent of the duct radius. The integration of this work into the noise model program developed by Dunn and Peart [13] was simplified by the conclusion that the maximum attentuation was independent of the boundary layer thickness over this range. The optimum wall lining as shown by the previous efforts in Reference 14 was sensitive to the boundary layer thickness.

A study of the numerical results of this previous effort permitted relationships between peak attenuation and frequency parameter to be established for cylindrical, annular, and rectangular ducts. These relationships were put in arrays as an alternative to the empirical arrays in the original program. As shown for the cylindrical duct in Reference 3, page 39, the least attenuated mode theory predicted a larger attenuation at low frequency than Dunn and Peart's empirical predictions and predicted a lower attentuation at high frequencies than the empirical. The difference at low frequencies was possibly associated with deviations from the assumed conditions which would cause measured attenuation to be less than that predicted. At high frequencies the attenuation predicted by the least attenuated mode theory was lower than the empirical because the theory was very conservative when a large number of modes propagated in the duct as happens at high frequencies. All of the other modes were attenuated more than the least attenuated mode on which the prediction was based.

For these reasons the least attenuated mode theory was suspect at high frequencies and other assumptions regarding how much of the sound energy was in each of the propagating modes were suggested.

EQUAL ENERGY THEORY INTEGRATION

The equal energy theory assumed that an equal portion of the total sound energy was in each propagating mode. Propagating modes were those with real phase velocities as defined in Equation (26). Since the α in Equation (26) was for hard walls

there was the possibility that another mode or two might propagate at high frequencies but the modes which barely propagated were highly attenuated and did not effect the results. At the highest value of the frequency parameter in the original program range there were 114 modes propagating.

Rather than finding the exact attenuation of every mode with the usual iterative process, the results of Section III were used to estimate the modal attenuations. These estimates were used to start the iterative process for the lightly attenuated modes which contribute most to final energy at the end of the duct. The attenuations of more heavily attenuated modes which have only a small contribution to the final energy were taken directly from the approximate results of the Section III analysis.

The attenuation of these modes with equal energy in each at the duct inlet was calculated from

$$E_o/E_i = \frac{1}{N} \sum_{i=1}^{N} e^{-kL\sigma_i} \tag{69}$$

or in decibels.

$$\text{Attenuation} = 10 \log_{10} E_o/E_i \tag{70}$$

Here E_o and E_i are the energies out and in the duct. The number of propagating modes is N and the attentuation constant σ_i is found from Equation (29) or an iterative solution. The reduced frequency based on duct length kL also appears.

From these results the predicted peak attenuation as a function of frequency parameter and normalized duct length, L/H, was found. An array containing this information was included in the noise prediction program as a second alternative to the empirical prediction of peak attenuation. This array of peak attenuation values as a function of y = HF/c and L/H is shown in Table 2. This table is used only under control option IMAm = 3 as detailed in the subsection entitled, "Modification Control".

EXTERNAL ATTENUATION MODIFICATION

The preceding two theories are by no means the only possible theoretical attenuation approaches. They do not consider variations of the duct lining along its length. They do not consider variations of duct cross-sectional area. They do not consider arbitrary distribution of the sound energy among the propagating modes. Numerical schemes such as the finite difference approaches in Section V can include these effects. Consequently, the noise prediction program was modified to permit the results of an external program like those of Section V to be used in the noise prediction.

TABLE 2

EQUAL ENERGY PEAK ATTENUATION ARRAY

Peak Attenuation Prog. Array 69z		-.4 .398	-.2 .632	0 1	.2 1.58	.4 2.51	.6 3.98	log HF/C HF/C
-1	.1	1.9	1.76	1.56	1.25	.79	.33	
-0.8	.158	3.0	2.73	2.31	1.80	1.17	.51	
-0.6	.251	4.8	4.2	3.4	2.56	1.63	.80	
-0.4	.398	7.6	6.4	5.0	3.6	2.25	1.24	
-0.2	.631	12.0	9.4	7.1	5.0	3.2	1.91	
0	1	18.9	14.0	10.1	7.0	4.6	2.9	
.2	1.58	29.9	21.2	14.7	10.0	6.7	4.4	
.4	2.51	47.1	31.7	21.0	14.3	9.7	6.6	
.6	3.98	74.1	47.2	30.5	20.4	13.9	9.7	
.8	6.31	117.	70.0	44.5	29.2	19.7	14.3	
1.0	10	183	109	66.5	42.7	28.6	20.8	

log L/H L/H

The approach to this modification was simply to bypass the internal attenuation process and to enter the externally computed attenuation of the desired duct directly as attenuation as a function of frequency. This was accomplished using existing control parameters and simply changing their range.

MODIFICATION CONTROL

The existing parameters LGMm and IMAm were used to control the new program modifications. As they existed prior to modification in Crawley, et al [15] the old usage was:

OLD PARAMETER USAGE

IMAm Specifies whether program calculates or used defines peak attenuation for each target frequency.
= 0 program calculates
= 1 user defines PLAm values

LGMm Specifies whether program calculates peak attenuation using lining geometry or user. Defined effective duct height and ratio of treatment length to effective duct height.
= 0 user inputs EDHm and ELOHm
= 1 user inputs R1Wm and TLm
(the = 1 option only if IMAm = 0)

Here PLAm, EDHm, ELOm, R1Wm, and TLm are defined in Reference [15]. As currently modified the new usage of these parameters is:

NEW PARAMETER USAGE

IMAm Specifies how the program calculates peak attenuation or user defines peak attenuations for each target frequency.
= 0 original empirical attentuation calculation
= 1 user specifies from 1 to 24 PLAm values and from 1 to 24 TFm values
= 2 least attenuated mode calculations
= 3 equal energy peak attenuation calculations

LGMm Specifies whether program calculates peak attenuation using annular, rectangular or cylindrical geometry and type of input required.
= 0 rectangular or annular geometry with inputs EDHm and ELOm required
= 1 cylindrical geometry with inputs R1Wm and TLm required
(LGMm = 1 option only if IMAm = 0, 2 or 3)

The modified program also keys on the number of attenuation values input under option IMAm = 1. If 24 attenuation

values are input, the attenuation at a specified frequency is independent of the attenuation at neighboring frequencies. If less than 24 attenuation values are input under option IMAm = 1 the program works as originally designed where a bandwidth array causes the attenuation at any frequency to be effected by the attenuation at neighboring frequencies.

SECTION VII

PROGRAM VERIFICATION

AIRCRAFT SELECTION

The aircraft selected for baseline noise studies and verification of the program modifications was the KC-135B. The standard version of this aircraft was powered by four TF33-P5 turbofan engines.

BASELINE NOISE DATA

With the help of Lt. Raymond Geiselhard, Mr. Gregory Hughes, and Mr. Robert Bunting of ASD the engine data required to run the noise prediction program for the KC-135B with four TF33-P5 turbojet engines was obtained. This data is shown for both takeoff and approach conditions in Table 3. The noise predictions were made with an aircraft Mach number of 0.224 at takeoff and 0.140 at approach.

Similar data was obtained for the CFM 56 engine. This data, shown in Table 4, did not include some of the core noise parameters because the core noise was not thought to be significant for this engine.

COMPARISON OF PREDICTIONS WITH DATA AND CORRECTIONS

TF33-P5 Noise Comparison and Correction

The TF33-P5 engines on the KC-135B aircraft was a standard configuration tested for noise by Speakman, et al [16] with the Aero Medical Research Laboratory at WPAFB. This data, shown in Table 5 was used to develop corrections to the prediction program to cause it to predict the sound pressure levels measured in these flight tests.

The correction applied was a function of frequency using the DPB(I) parameter from the programs user's manual. [15] The program was corrected so that the difference between the prediction and measured noise for take-off and the same difference for approach averaged to near zero. Actually this average difference was less than one dB for 20 of the 24 frequencies. The corrections were applied to the jet noise portion of the program for frequencies less than 1000 Hz and to the fan noise portion of the program for frequencies of 1000 Hz or more. These corrections are shown for the TF33-P5 engines in Table 5 also. The corrections are as large as 25.3 dB near the blade passage frequency.

TABLE 3

ENGINE DATA FOR NOISE PREDICTION
DATA FOR KC-135B WITH TF33 P5 ENGINES

Ambient Standard Pressure 59° F

	Takeoff	Approach	Program Parameter
JET NOISE DATA			
Primary jet nozzle exit area - ft^2	3.70	3.70	API
Primary jet mass flow rate - lbm/s	206.7	135.6	WPI
Primary exhaust velocity returned to nozzle - ft/s	1663.	1020.	VPI
Secondary jet nozzle exit area - ft^2	3.65	3.65	AS2
Secondary jet mass flow rate - lbm/s	292.1	235.	WS2
Secondary exhaust velocity returned to nozzle - ft/s	1095.	861.	VS2
Airspeed - knots	250	160	
FAN NOISE DATA			
Pressure ratio of 1st fan stage	1.23	1.064	FPR45(1)
Pressure ratio of 2nd fan stage	1.18	1.021	FPR45(2)
No. blades of 1st fan stage	34	34	NB45(1)
No. blades of 2nd fan stage	32	32	NB45(2)
Fan rotor RPM	6540	5190	RNI45
Rotor/stator spacing 1st stage (as percent of rotor blade axial chord)	53.68	53.68	RSS45(1)
Rotor/stator spacing 2nd stage	83.33	83.33	RSS45(2)
Rotor diameter - ft	4.184	4.184	DIAM4(1,2)
Fan exit area - ft^2	5.29	5.29	AREA5(1,2)
Relative tip Mach No.	1.17	.83	RTS45
Fan press. ratio at 1.025 tip	1.6	1.6	CFPR4
CORE AND TURBINE NOISE DATA			
Combustion corr. mass flow rate - lbm/s	30.1	30.4	CMF3
Total turbine pressure ratio, P_i/P_θ	7.04	6.04	PP3
Combustion exit temperature - °R	2105.	1720.	TT3
Turbine RPM	6540.	5190.	SS3
Turbine outlet temperature	1950.	1125.	TU3
Turbine tip dia. last stage - ft	3.091	3.091	DT3
No. blades in last turbine stage	80	80	BN3
Stator/rotor spacing - % of stator chord	23.9	23.9	CS3
Primary mass flow - lbm/s	208.7	137.6	PMF3

TABLE 4

ENGINE DATA FOR NOISE PREDICTION
DATA FOR KC-135B WITH CFM 56 ENGINES

Ambient Standard Pressure 59° F

	Takeoff	Approach	Program Parameter
JET NOISE DATA			
Primary jet nozzle exit area - ft^2	4.02	4.02	API
Primary jet mass flow rate - lbm/s	117.4	37.7	WPI
Primary exhaust velocity returned to nozzle - ft/s	1259.2	383.2	VPI
Secondary jet nozzle exit area - ft^2	3.65	3.65	AS2
Secondary jet mass flow rate - lbm/s	694.5	321.0	WS2
Secondary jet exhaust velocity returned to nozzle - ft/s	864.2	396.6	VS2
Airspeed - knots	250	160	
FAN NOISE DATA			
Pressure ratio of 1st fan stage	1.23	1.064	FPR45(1)
Pressure ratio of 2nd fan stage	1.18	1.021	FPR45(2)
No. blades of 1st fan stage	34	34	NB45(1)
No. blades of 2nd fan stage	30	30	NB45(2)
Fan rotor RPM	4594	2098	RN145
Rotor/stator spacing 1st stage (as percent of rotor blade axial chord)	120	120	RSS45(1)
Rotor/stator spacing 2nd stage	122	122	RSS45(2)
Rotor diameter - ft	4.25, 4.01	4.25, 4.01	DIAM4(1,2)
Fan exit area - ft^2	5.35, 5.25	5.34, 5.25	AREA5(1,2)
Relative tip Mach No.	.913	.4	RTS45
Fan press. ratio at 1.025 tip	1.3	1.3	CFPR4

TABLE 5

NOISE DATA FOR THE KC-135B
SLANT RANGE 1000 ft

Frequency (I)	Measured SPL Takeoff	Measured SPL Approach	Jet Noise Corrections DPB(I) db	Fan Noise Corrections DPB(I) dB
50	78.3	69.6	14.7	0
63	73.6	66.3	34.4	0
80	76.5	68.7	26.7	0
100	87.5	75.6	-.9	0
125	91.9	81.9	-11.5	0
160	93.2	82.8	-12.7	0
200	87.1	76.1	0	0
250	90.7	79.9	-8.5	0
315	92.9	79.2	-11.1	0
400	91.1	80.3	-12.5	0
500	90.2	78.8	-11.0	0
630	90.7	79.5	-14.0	0
800	89.2	77.4	-12.8	0
1000	88.2	78.6	0	-7.6
1250	87.5	83.1	0	-10.4
1600	87.2	78.4	0	-7.7
2000	87.2	81.3	0	-10.8
2500	88.1	97.5	0	-25.3
3150	97.2	91.7	0	-14.8
4000	90.8	79.7	0	-7.6
5000	80.3	83.9	0	-17.1
6300	81.0	77.6	0	-9.5
8000	74.7	73.3	0	-10.5
10000	67.0	62.1	0	-20.1

CFM 56 Noise Comparisons and Correction

The CFM 56 predictions were corrected based on static test data taken in a 100 ft diameter circle. This work was done in cooperation with Mr. Ronald Tagg of ASD as part of a previous Propulsion Laboratory contract. The correction was applied as a function of angle from the engine centerline. This was done via the DOB(I) parameter of the program users manual.[15] The resultant corrections are shown in Table 6. The corrections are as large as 11.6 dB in the critical region near 90 degrees from the engine centerline.

BASELINE AND LINED NOISE PREDICTIONS

The TF33—P5 engined KC-135B data were input to the noise prediction program for four duct lining conditions. They were:

1. Hard walled ducts.
2. Three foot lining optimized for the blade passage frequency (3488 Hz) as inlet duct.
3. Six foot lining optimized at 3200 Hz as inlet duct.
4. Six foot lining with splitter optimized at 3200 Hz as inlet duct.

Lining number 2 above was run using the equal energy option. The others were run using the original program duct attenuation predictions. The linings effect during approach was much greater than their effect during take-off because the take-off was dominated by jet noise. The jet noise prediction was not effected by inlet linings. The effects of the linings during approach is shown in Figure 4. This figure shows that appoach noise is almost all at blade passage frequency for this engine. The splitter lining caused about a 7 dB noise reduction. The three foot lining with no splitter had an almost negligible efect. This is because large ducts at this high frequency have low attenuation. The splitter, by dividing the effective duct size in half, causes the product of duct size and frequency to b small enough that the lining is more effective.

The CFM 56 engined KC-135B data were input to the noise prediction program for four duct lining conditions also. They were:

1. Hard walled ducts.
2. Three foot linings optimized 50% at 2500 Hz and 50% at 3200 Hz for both fan inlet and exhaust.
3. Six foot linings optimized 50% at 1260 Hz and 50% at 2500 Hz for both fan inlet and exhaust.
4. Six foot linings optimized 90% at 1260 Hz and 10% at 2500 Hz for both fan inlet and exhaust.

Lining number 2 above was run using the equal energy option. Lining number 4 was run using the least attenuated mode option. The others were run using the original program duct attenuation predictions. Again the effects of the linings were

TABLE 6

NOISE PREDICTION CORRECTIONS
FOR THE CFM 56

Angle from Engine Centerline (I)	Correction dB DOB(I)
10	-14.3
20	- 5.2
30	- 3.7
40	- 3.7
50	- 1.4
60	3.2
70	5.7
80	8.0
90	10.6
100	11.4
110	11.6
120	9.0
130	5.8
140	5.8
150	5.8
160	.7
170	- 9.3

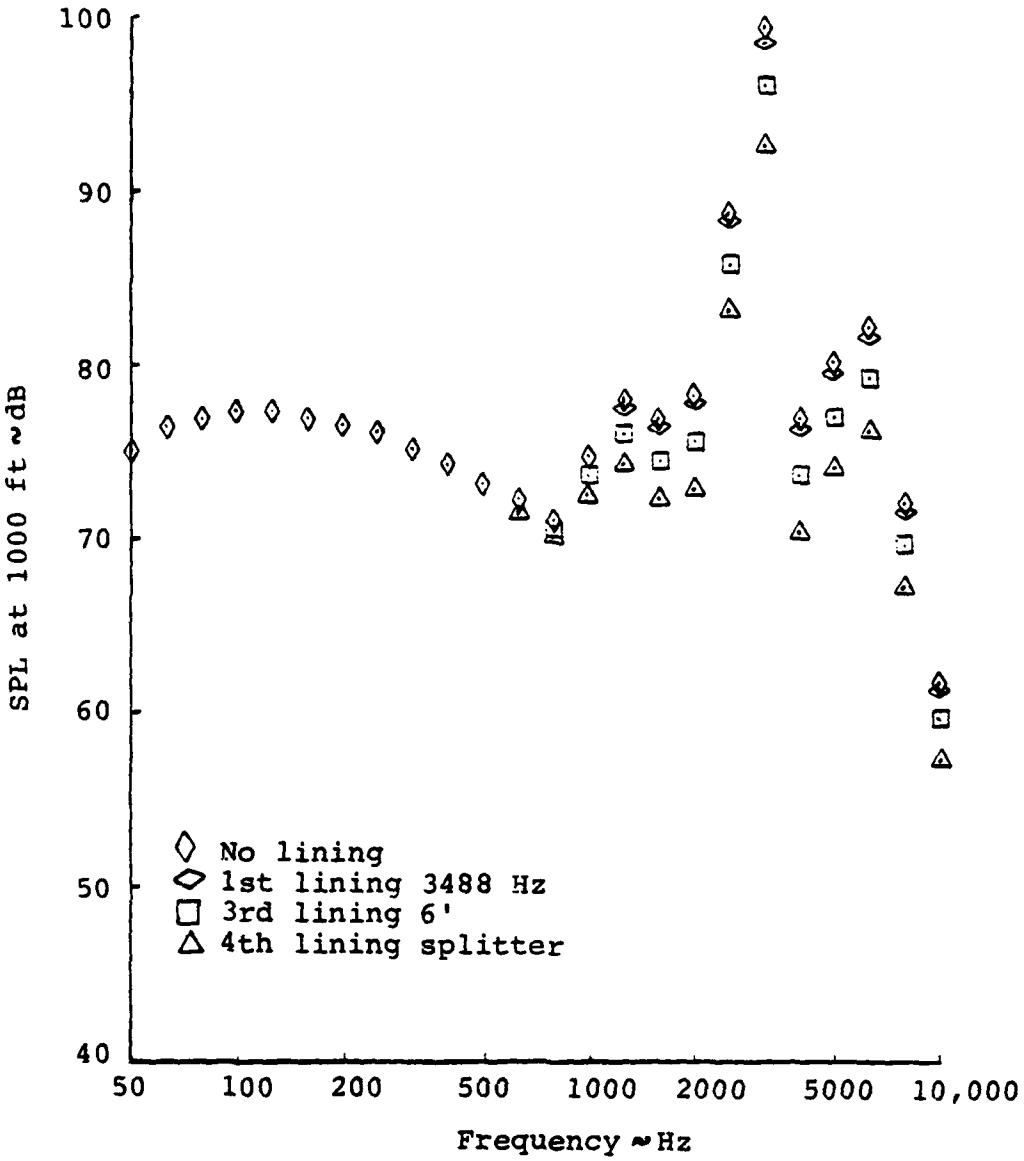

Figure 4. TF33-P5 Approach

significant only during approach conditions. These effects are shown in Figure 5. This figure shows that the fourth lining was predicted to the the most effective and that it would be expected to reduce the overall sound pressure level by about 8 dB. This lining was run with the least attenuated mode option which predicts less attenuation than the other possible options at these frequencies. The linings were more effective in this engine than for the TF33-P5 because the dominate frequencies were lower which permits the linings to have a greater attenuation.

PHYSICAL LINING CHARACTERISTICS

The lining predictions for the CFM 56 were based on optimized linings at the fan blade passage frequency and its first harmonic. The physical characteristics of these linings can be obtained by utilizing the lining impedance models of Section II. The perforated sheet model was used with the assumption of a seventh power boundary layer velocity profile of 1/2 inch thickness. This thickness corresponds to a momentum thickness of about 10% of the total boundary layer thickness. The input to the lining model was:

Perforated sheet thickness	.040 inches
Static air temperature	540°R
Static air pressure	14.7 psi
Frequency	1260 Hz
Sound pressure level	160 dB
Flow Mach number	-.5
Boundary layer momentum thickness	.05 inches
Normalized lining resistance $R/\rho c$	5.68
Normalized lining reactance $X/\rho c$	-8.51

The resultant lining optimized for the blade passage frequency of 1260 Hz had a depth of .218 inches with a percent open area of about 5%. At 2600 Hz the optimum lining had a depth of .192 inches and a percent open area of about 27%. A no boundary layer analysis at this frequency gave a core depth of .453 inches with about 2% open area. This sensitivity of the optimum lining open area to boundary layer parameters was the subject of Reference 14. For these linings the effect of the linings on aircraft performance would be minimal because the backing depths would not significantly change the size of the engine. A procedure for computing these effects on performance has been developed in coordination with ASD personnel. The procedure was not actually carried out for these linings because of the small effect anticipated. Linings designed for lower frequency noise suppression would have larger backing depths with significant effects on engine size and consequently performance.

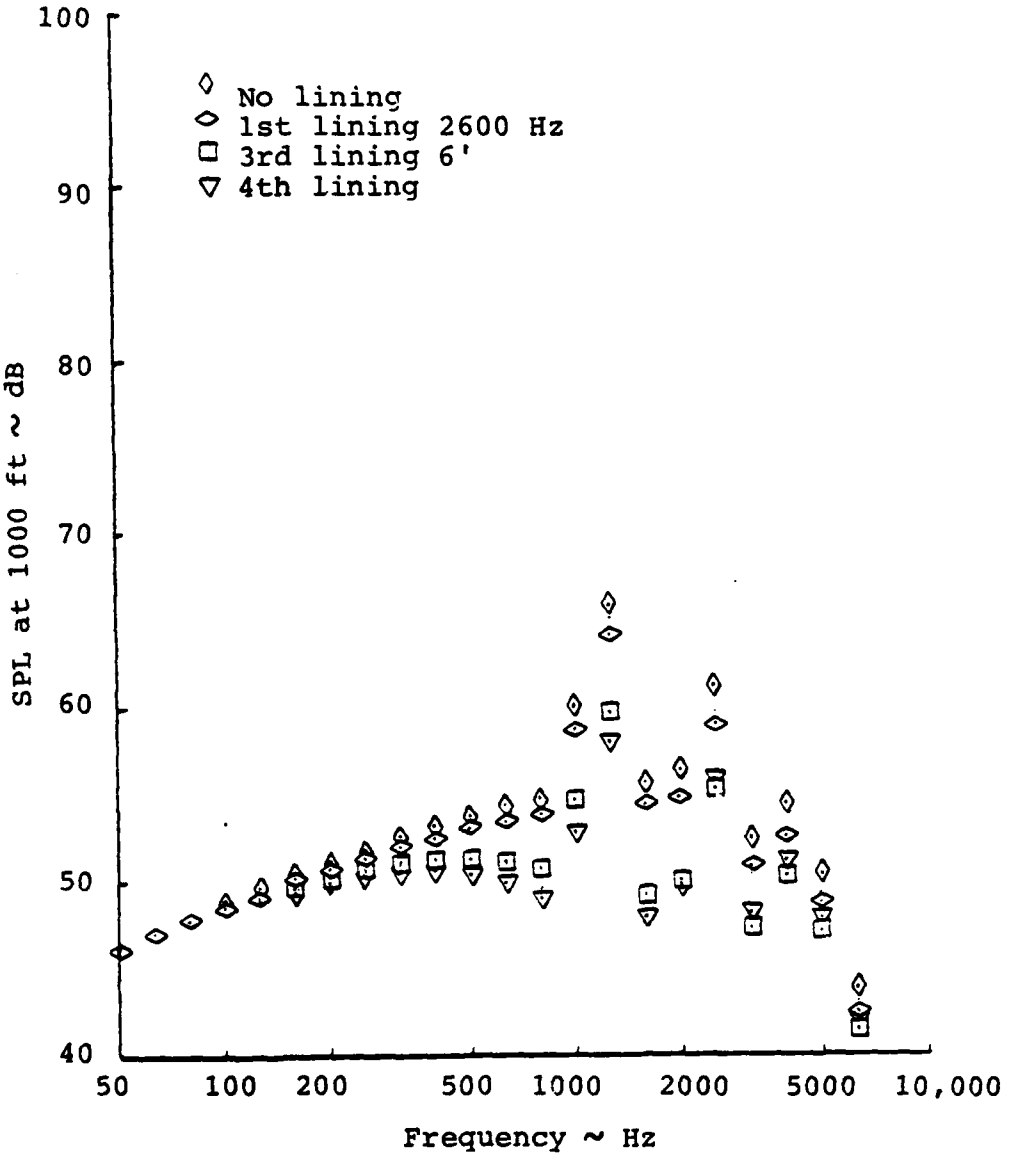

Figure 5. CFM 56 Approach

SECTION VIII

DISCUSSION AND RECOMMENDATIONS

The lining impedance models of Section II represent an empirical model relating physical and acoustic parameters. The boundary layer effects must be considered as tentative until theoretical studies relating hole diameter, shear velocity, and other details of the flow field near the holes are incorporated into the model. These theoretical studies have been in progress for years without significant contributions. The Section II model should, however, be adequate for a first pass estimate of size effects as required for a good aircraft performance computation.

The approximate sound propagation parameters developed in Section III permit a physically meaningful estimate for a problem where a more exact numerical solution is difficult. It is recommended that this approach be extended to: (1) boundary layer effects via an impedance change across the boundary layer as approximated by an Eversman and Beckemeyer [17] type expansion, and (2) variable area ducts where ray acoustics might be a natural way to approximate the area variation effects.

Sheared flow orthogonality proved to be an area where considerable effort in seeking perturbation solutions to the governing equations produced no results. This interaction of the flow field with the acoustics is a field of study which is related to basic research in turbulence and represents an important problem area. It is recommended that numerical solutions of these partial differential equations be used to study this problem further.

The study of sound propagation in variable area ducts (Section V), produced some satisfying developments. The capability to prescribe any cylindrical or annular axisymmetric geometry along with any axial variation of wall impedance permits an impressive range of ducts to be analyzed. The bullet nosed inlet is a good example of a geometry of practical importance. It is recommended that this numerical technique be refined and used in a parametric study involving axial impedance changes in wall impedance.

With flow included the governing partial differential equations do not permit an easy reduction to a single variable as in the no flow variable area duct case. Difficulty with instabilities as time was marched forward made progress difficult for the numerical solution attempted. Although stable techniques were found they did not permit the range of variables sought. It is recommended that: (1) Apparent problems in prescribing the time varying inlet condition be investigated further. This apparent problem can even be seen in the no flow

results for the bullet nose inlet where the first interior imaginary pressure seems to be in error. For the no flow case the system stability was enough to overcome this problem and permit the solution to approach a steady-state value. For the flow case this problem may be causing the instabilities. (2) Extend the flow solution which was well behaved to include compressibility effects. This improvement is seen as only a minor change in a portion of the problem which is giving no difficulty.

The noise/performance model integration incorporated the basis axially uniform lining results. It is recommended: (1) to incorporate the results of a multi-segmented study as another option, (2) to pursue studies of multi-segmented variable area ducts as a long range goal, and (3) to continue the policy of a separate noise model with tools to convert its output to performance related input. This permits the flexibility to meet varying needs.

The program verification consists of a verification that the program modifications work and of a study of possible acoustic implications of lining either the TF33-P5 or the CFM 56 engined KC-135. The studies showed that the approach noise could be reduced significantly with the CFM 56 engine by duct linings. The TF33-P5 engine noise, however, was difficult to attenuate because of its high frequency. With the best lining tried the CFM 56 engined aircraft was more than 30 dB quieter than the TF33-P5 engined aircraft on approach. This is with a splitter in the TF33-P5 inlet.

REFERENCES

1. Armstrong, D. L., Acoustic Grazing Flow Impedance Using Waveguide Principles, Boeing D3-8684, Dec. 1971.

2. Rice, E. J., Heidman, M. F., and Sofrin, T. G., "Modal Propagation Angles in a Cylindrical Duct with Flow and Their Relation to Sound Radiation," AIAA Paper No. 79-0183, Jan. 1979.

3. Schauer, J. J., Hoffman, E. P., and Guyton, R. E., Sound Transmission Through Ducts, AFAPL-TR-78-25, May 1978.

4. Rice, E. J. and Heidman, M. F., "Modal Propagation Angles in a Cylindrical Duct with Flow and Their Relation to Sound Radiation," AIAA Paper No. 79-0183, Jan. 1979.

5. Baumeister, K. J., Numerical Techniques in Linear Duct Acoustics - A Status Report, NASA-TM-81553, Nov. 1980.

6. Baumeister, K. J., Time Dependent Difference Theory for Noise Propagation in a Two-Dimensional Duct, NASA-TM-79298, Jan. 1980.

7. Baumeister, K. J., Time Dependent Difference Theory for Sound Propagation in Axisymmetric Ducts with Plug Flow, NASA-TM-81501, June 1980.

8. Quinn, D. W., "A Finite Different Method for Computing Sound Propagation in Nonuniform Ducts," AIAA Paper No. 75-130, Jan. 1975.

9. Quinn, D. W., "A Finite Element Method for Computing Sound Propagation in Ducts Containing Flow," AIAA Paper No. 79-0661, 1979.

10. Eversman, W., Astley, R. J., and Thanh, V. P., "Transmission in Nonuniform Ducts - A Comparative Evaluation of Finite Element and Weighted Residuals Computational Schemes," AIAA Paper No. 77-1299, Oct. 1977.

11. Petty, J. S., Research in Computational Fluid Dynamics, ARL-TR-75-0209, June 1975.

12. Reddick, H. W. and Miller, F. H., Advanced Mathematics for Engineers, 3rd Edition, John Wiley & Sons, N.Y., 1955.

13. Dunn, D. G. and Peart, N. A., Aircraft Source and Contour Estimation, NACA-CR-114649, July 1973.

14. Schauer, J. J. and Hoffman, E. P., "Optimum Duct Wall Impedance-Shear Sensitivity," AIAA Paper No. 75-129, Jan. 1975.

15. Crowley, K. C., Jaeger, M. A., and Meldrum, D. F., Aircraft Noise Source and Contour Computer Programs User's Guide, NACA-CR-114650, July 1973.

16. Speakman, J. D., Powell, R. G., and Lee, R. A., Community Noise Exposure Resulting from Aircraft Operations, Vol. 2, Acoustic Data o n Military Aircraft: Air Force Bomber/Cargo Aircraft, AMRL-TR-73-110, Vol. 2, Nov. 1977.

17. Eversman, W. and Beckemeyer, R. J., "Transmission of Sound in Ducts with Thin Shear Layers - Convergence to the Uniform Flow Case," Journal of the Acousticl Society of America, Vol. 52, No. 1, pp. 216-220, 1972.